THE JOURNAL OF PHYSICAL CHEMISTRY B

Article

pubs.acs.org/JPCB

Atomistic Simulations of a Multicomponent Asymmetric Lipid Bilayer

Anirban Polley,[†] Satyavani Vemparala,[‡] and Madan Rao*[,†,§]

[†]Raman Research Institute, C. V. Raman Avenue, Bangalore 560 080, India

[‡]The Institute of Mathematical Sciences, CIT Campus, Chennai 600 113, India

[§]National Centre for Biological Sciences (TIFR), Bellary Road, Bangalore 560 065, India

Supporting Information

ABSTRACT: The cell membrane is inherently asymmetric and heterogeneous in its composition, a feature that is crucial for its function. Using atomistic molecular dynamics simulations, the physical properties of a 3-component asymmetric mixed lipid bilayer system comprising an unsaturated POPC (palmitoyloleoylphosphatidylcholine), a saturated PSM (palmitoylsphingomyelin), and cholesterol are investigated. Our simulations explore both the dynamics of coarsening following a quench from the mixed phase and the final phase-segregated regime obtained by equilibrating a fully segregated configuration. Following a quench, the membrane quickly enters a coarsening regime, where the initial stages of liquid ordered, l_o, domain formation are observed. These growing domains are found to be highly enriched in cholesterol and PSM. Consistent with this, the final phase-segregated regime contains large l_o domains at equilibrium, enriched in cholesterol and PSM. Our simulations suggest that the cholesterol molecules may partition into these PSM-dominated regions in the ratio of 3:1 when compared to POPC-dominated regions. PSM molecules exhibit a measurable tilt and long-range tilt correlations within the l_o domain as a consequence of the asymmetry of the bilayer, with implications to local membrane deformation and budding. Tagged particle diffusion for PSM and cholesterol molecules, which reflects spatial variations in the physical environment encountered by the tagged particle, is computed and compared with recent experimental results obtained from high-resolution microscopy.

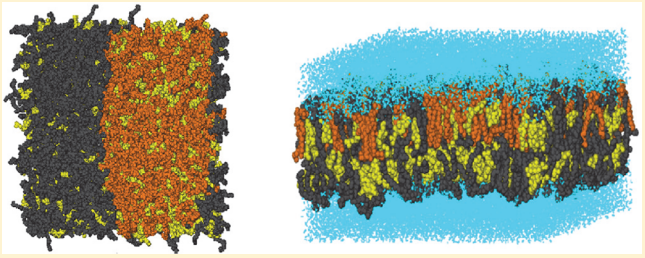

INTRODUCTION

The cell membrane is characterized by both lateral and transverse lipid heterogeneity, an aspect of significant functional consequence.[1] Transverse lipid heterogeneity is maintained actively by the cell, making the cell bilayer intrinsically asymmetric. Lateral lipid heterogeneities called "rafts",[2,3] which are ternary mixtures of sphingomyelin (PSM), phosphatidylcholine (PC), and cholesterol (Chol) molecules, have been implicated in a variety of cellular processes including signaling and endocytosis, even though the nature of these functional cellular rafts is still a matter of contention.[4−7] Asymmetry in bilayers can arise both in terms of difference in constituent lipids or in number of lipid molecules in both leaflets. In spite of this obvious lateral/transverse compositional heterogeneity, except for a few seminal studies,[8] most in vitro investigations of multicomponent artificial membranes[9−11] have been done on symmetric bilayers. Further, most of the atomistic simulations of model cell membrane mimics have been carried out on systems which have either lateral heterogeneity[12] or transverse asymmetry[13−15] but rarely both. There have, however, been a few studies using coarse-grained simulations[16−18] and continuum Landau theories[19−21] that address the role of interbilayer coupling in equilibrium physical properties and domain growth.

While early simulations of model membranes consisted only of a single-component PC bilayers,[22−24] later simulations have incorporated more than one lipid component, in particular cholesterol.[25] Following the "raft proposal" of the importance of PSM molecules in raft formation, an increasing number of simulations with PSM molecules[26] have been carried out. These simulations include detailed comparisons between mixtures of PSM and Chol and PC and Chol.[12,27−31] Finally, simulations on asymmetric bilayers have also been reported. A simulation study by Bhide et al.[32] was performed on systems consisting of PSM and Chol molecules in upper leaflet and SOPS and Chol molecules in the lower leaflet, with equal number of phospholipids in both the leaflets. Comparisons between each leaflet of the asymmetric bilayer with corresponding simulations of symmetric bilayers showed no significant differences in their physical properties.

In this paper, the equilibrium properties and dynamics of coarsening of a multicomponent asymmetric (both lateral and transverse) bilayer using atomistic molecular dynamics (MD) simulations are studied. Specifically, the physical properties of a 3-component asymmetric lipid bilayer comprising an unsatu-

Received: April 6, 2012
Revised: October 16, 2012
Published: October 22, 2012

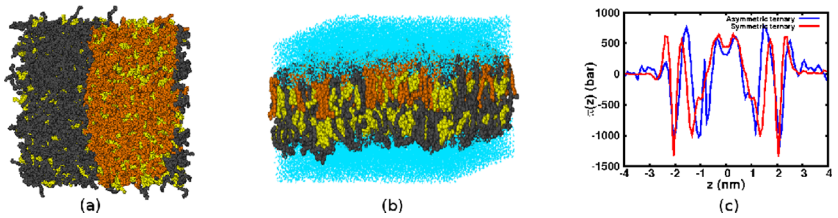

Figure 1. (a) Snapshot (top view) at the end of the simulation starting from a fully segregated configuration of the ternary system POPC (gray), PSM (orange), and Chol (yellow) forming a stable asymmetric bilayer in water (not shown for visual clarity). (b) Snapshot (side view) at the end of the simulation starting from a homogeneous mixed configuration of the same asymmetric bilayer in water (cyan). (b) Lateral pressure profiles $\pi(z)$ as a function of position across the bilayer, for the ternary asymmetric bilayer (blue), and the ternary symmetric bilayer (red). (Lateral pressure profiles for symmetric bilayers made of POPC and POPC+Chol shown in Supporting Information, Figure S1.) See Results and Discussion for definition.

rated POPC, saturated PSM and Chol molecules, which exhibits lateral compositional heterogeneities in the form of liquid ordered (l_o)−liquid disordered (l_d) domains, thought to represent the characteristic lipid composition of rafts on the cell membrane, are investigated. In addition to studying a variety of order parameters, and their correlations and spatial distribution, transport properties of the component lipid molecules are also studied. Our study suggests that the presence of lateral heterogeneities in the bilayer can potentially affect the molecular diffusion at short time scales, which may be of relevance to molecular diffusion at the cell surface. However, lipid-based lateral heterogeneities on the cell surface are likely to be small and below optical resolution; it is only recently that advances in high-resolution single-particle tracking (SPT)[33,34] allow one to measure subtle changes in diffusion characteristics as molecules move across the heterogeneous cell surface. In addition, the transverse asymmetry would suggest that the diffusion characteristics of the molecule is different in the two leaflets of the bilayer. Correlations between the local physical environment and the tagged particle diffusion are also investigated in this paper.

MATERIALS AND METHODS

Two bilayer model systems have been simulated: (A) a symmetric three-component bilayer consisting of 170 POPC, 171 palmitoylsphingomyelin (PSM, saturated lipid), and 171 Chol whose ratio is 1:1:1 in each leaflet, for a total 1024 lipids and (B) an asymmetric bilayer with a composition of 170 POPC, 168 PSM, and 171 Chol whose ratio is roughly 1:1:1 in the upper leaflet and 256 POPC and 256 Chol whose ratio is 1:1 in the lower leaflet, for a total 1024 lipids. Two control systems have also been simulated, which are (C) a symmetric one-component bilayer made up of a total 128 pure POPC and (D) a symmetric two-component bilayer made up of a total 64 POPC and 64 Chol whose ratio is 1:1 in both leaflets.

The force field parameters for POPC were taken from the previously validated united-atom description (Tielman and Berendsen[35]), whereas for PSM and Chol parameters from works of Niemela et al.[12] were used. Water was simulated by the simple point charge (SPC) model[36] and PACKMOL[37] was used to generate the initial configurations of all the bilayer systems and hydrated with water in the ratio of 1(lipid):32 (water).

All atomistic MD simulations were performed at a temperature T = 296 K, which lies between the main transition temperatures of POPC (T_m = −2.9 ± 1.3 °C)[38] and PSM (T_m ≈ 41.4 °C)[39] and right in the middle of the l_o−l_d phase coexistence region of the symmetric ternary system.[40] GROMACS (http://www.gromacs.org)[41] software was used to integrate the equations of motion with a time step of 2 fs. To avoid bad contacts arising from steric constraints during initialization, all bilayer systems were subjected to steepest descent minimization initially. The systems were then simulated for 50 ps in the NVT ensemble using a Langevin thermostat. Subsequently, each system was simulated in the NPT ensemble (T = 296 K, P = 1 atm) using a Berendsen thermostat and semi-isotropic pressure coupling with compressibility 4.5 × 10^{-5} bar^{-1} for 220 ns (for the asymmetric ternary system B) and for 100 ns (for symmetric ternary system A) and for 100 ns (for the single- and two-component systems C and D). The long-range electrostatic interactions were incorporated by the reaction-field method (with cutoff, r_c = 2 nm) and a cutoff of 1 nm was used for the Lennard-Jones interactions, the efficacy of this method has been discussed earlie.[12,42] Lipid system parameters such as deuterium order parameter and mean thickness were monitored throughout the simulations to ensure that the system is well equilibrated. All the reported results are computed over last 20 ns unless otherwise stated.

The two model systems A and B have been simulated starting from two sets of initial conditions: (i) where the components in each leaflet are homogeneously mixed and (ii) where the ternary components are completely phase segregated (Figure 1a,b).

Details of the measurement procedure are provided below. The lateral pressure profiles in the bilayer were measured using Irving−Kirkwood contour, and the bilayer was divided by 0.1 nm thick slabs. Pairwise forces were calculated by rerunning the trajectory with cutoff 2 nm for electrostatic interactions. The LINCS algorithm were used to constrain the bond lengths,[43] and the SETTLE algorithm were used to keep the water molecules rigid[44] so that integrator time step of 2 fs could be used. The pressure profiles were generated from trajectories over 20 ns using SHAKE algorithm[45] to constrain bond lengths.

The thickness of the bilayer membrane was calculated from head-to-head (P-atom of POPC and PSM) distance of the lipids in the upper and lower leaflets of the bilayer. To avoid errors coming from the possible misalignment of the lipids in two leaflets, the positions of the headgroup (P-atom) of the lipids in the two leaflets were binned in xy-plane separately. Thus, the local bilayer thickness is constructed using x−y grids for the upper and lower leaflet of the bilayer, with grid size = 1.95 nm. An average over the z-coordinates of the phosphorus atom in the head groups of POPC and PSM within each x−y grid is then performed. The difference between the z-coordinates corresponding to the same x−y grid of the two leaflets gives the local bilayer thickness.

dx.doi.org/10.1021/jp3032868 | J. Phys. Chem. B 2012, 116, 13403−13410

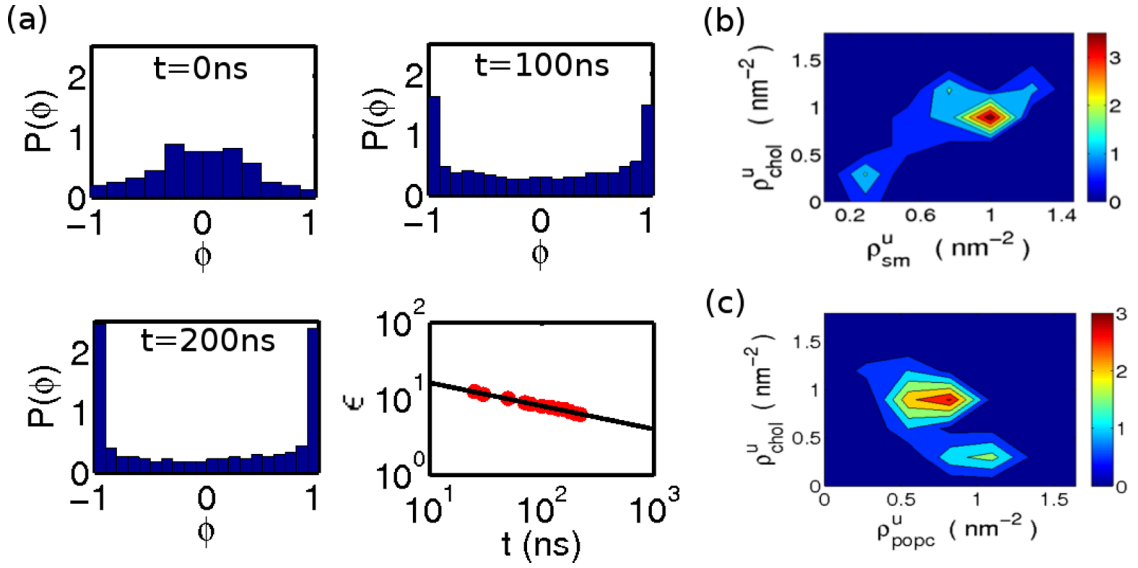

Figure 2. (a) Probability distribution $P(\phi)$ (normalized) of the order parameter $\phi = (\rho_{SM} - \rho_{POPC})/(\rho_{SM} + \rho_{POPC})$, where ρ_{PSM} and ρ_{POPC} are the concentrations of PSM and POPC, respectively, in the asymmetric ternary bilayer. Its time dependence from $t = 0-200$ ns, shows that the system, initially prepared in the mixed state ($\phi = 0$), has coarsened into PSM-rich ($\phi = 1$) and POPC-rich ($\phi = -1$) domains separated by sharp interfaces. The last panel shows the dependence of the energy density ε with time. The data (red filled circles) suggests that ε goes as a power law, $\varepsilon \sim t^{-0.3\pm0.15}$ (fitted line), with an exponent consistent with dynamical scaling, $z = 3$ (see text). (b) Joint probability distribution (color bar) of the concentration (in units of number/nm^2) of (b) PSM and Chol and (c) POPC and Chol, coarse-grained over [1.73 nm]^2 in the upper leaflet and averaged over 20 ns. Red shows the highest joint probability and blue the lowest. Note the strong correlation (anticorrelation) between PSM−Chol (POPC−Chol), respectively. The figures clearly show an enrichment of cholesterol in PSM-enriched domains by a ratio 3:1.

The deuterium order parameter (S) values were calculated from the selected carbon atoms positions of the PSM and POPC lipid chains. In our atomistic MD simulations, S is defined for every selected CH_2 group in the chains as $S \equiv {}^1/_2\langle 3\cos^2\theta - 1\rangle$, where θ is the angle between a CH-bond and the normal to the plane of the membrane (z-axis). Since we have used a united atom model description in our simulation, we have to reconstruct the CH bond from the positions of successive CH_2 groups, assuming tetrahedral geometry of the CH_2 groups. For each molecule, an averaging is done over the two bonds in each CH_2 group. This is then coarse-grained (binned) over a spatial scale of 1.56 nm and time scale of 20 ns. For the present purposes, carbon atoms 5−7 were selected from each acyl chains (corresponding to palmitoyloleoyl chains of POPC, and palmitoylsphingosine of PSM). This choice of carbon atoms best characterizes the acyl chain rigidity induced by the proximal cholesterol.[12]

RESULTS AND DISCUSSION

To make sure that a stable, surface-tension-less asymmetric bilayer is being simulated, the forces, torques, and surface tension of the bilayer are computed from the local stress tensor $\sigma_{ij}(x,y,z) = (1/v)\sum_\alpha f_i^\alpha r_j^\alpha$, where f_i^α is the ith component of the force on the αth particle due to all other particles within a coarse-grained volume $v = [0.1\text{ nm}]^3$. The net force $F_i = \int \partial_k \sigma_{ik}\, dv$ and its first moment (related to the torque) $M_{ik} = \int (\partial_l \sigma_{il} x_k - \partial_l \sigma_{kl} x_i)\, dv$ for the bilayer were computed and both force and torque balance, $F_1 = 0.29 \pm 3.34$, $F_2 = -2.56 \pm 2.09$, and $F_3 = -2.16 \pm 3.2$, in units of nN, and $M_{12} = 0.77 \pm 0.428$, $M_{13} = -8.83 \pm 2.04$, and $M_{23} = -13.303 \pm 1.67$, in units of nN·nm, were achieved, suggesting a mechanically stable asymmetric bilayer. These are comparable to the corresponding values for the symmetric bilayers (see Supporting Information). The membrane surface tension is calculated as $\gamma = \int \pi(z)\, dz$, integrated over the width of the bilayer, where $\pi(z)$ is the lateral pressure, given by $\pi(z) = {}^1/_2(\bar{\sigma}_{xx}(z) + \bar{\sigma}_{yy}(z) - \bar{\sigma}_{zz}(z))$,[46,47] resulting in a value of $\gamma = -0.0018 \pm 0.0301$ bar·nm, essentially a "zero" surface tension bilayer. More details of time dependence of net forces, their moments and surface tension are provided in the Supporting Information, Figure S2. A snapshot of the equilibrium bilayer configuration of the asymmetric membrane is shown in Figure 1a,b. In Figure 1c, the pressure profiles of symmetric and asymmetric bilayers are shown for comparison. In contrast to the asymmetric bilayer, the symmetric bilayer exhibits a symmetric pressure profile about the midplane. On the other hand, the pressure profile of the asymmetric bilayer shows larger spatial oscillations.

As mentioned in Materials and Methods, the simulations on systems A and B have been carried out from two sets of initial conditions. One set of initial conditions is where the composition is *homogeneously mixed* in each leaflet; with this as the configuration at time $t = 0$, the membrane was quickly seen to enter a coarsening regime (as explicitly demonstrated below), with l_o domains, enriched in cholesterol and PSM, growing slowly (algebraically) in time. We will see below that the dynamics by which domains grow corresponds to the well-known coarsening dynamics of phase segregation,[48] which implies that there is both local equilibrium and an *approach toward global equilibrium*. The time taken to attain global equilibrium, however, gets larger as the system size gets larger: in all runs on system B we have gone up to 220 ns. The other set of initial conditions is where the composition is completely segregated; with this as initial condition, the configuration was seen to very quickly attain equilibrium phase segregation with large domain coexistence. We have used the time dependence of the area per lipid (Supporting Information, Figure S3) to test for equilibration (≈20 ns) and have run the simulation for times longer than that.

dx.doi.org/10.1021/jp3032868 | J. Phys. Chem. B 2012, 116, 13403−13410

Both these initial conditions are important. The first one tells us that the homogeneous mixed phase is unstable, and the coarsening dynamics suggests that it *approaches* global equilibrium. The second tells us that the global segregated equilibrium phase is stable. The bulk properties at late times from these two initial conditions are expected to be consistent, as explicitly demonstrated below. In each of the subsections below, we have presented results from both these initial conditions.

Lipid Composition. At the temperature and overall lipid composition under consideration, the homogeneous mixed phase of both the asymmetric and symmetric bilayers is unstable and exhibits definite features of phase separation between POPC-rich and PSM-rich domains (Supporting Information, Figures S4 and S5); in the asymmetric bilayer phase segregation occurs in the upper leaflet alone, while the composition in the lower leaflet remains homogeneous. To show that the bilayer is undergoing phase separation toward a complete phase-segregated configuration, the theory of dynamical coarsening,[48] which deals with the study of the dynamics of domain formation starting from a complete disordered phase, is used. In simulations starting from an initial mixed state, it is found that the system quickly phase segregates; at early times the domain sizes are small and grow over the simulation time, 220 ns. To demonstrate that at these times the system enters a nonlinear coarsening regime (a hallmark of phase segregation leading to an eventual completely phase-segregated state), we have computed the time dependence of (i) the probability distribution $P(\phi)$ of the order parameter $\phi = (\rho_{SM} - \rho_{POPC})/(\rho_{SM} + \rho_{POPC})$ of the asymmetric bilayer membrane, model B (where $\rho_{SM/POPC}$ is the local density of PSM/POPC), and (ii) the energy density $\varepsilon = E/V$, where the energy $E \propto \int d^2r(\nabla\phi)^2$. In Figure 2a, we have shown the $P(\phi)$ of the asymmetric ternary bilayer at initial (t = 0 ns), final (t = 200 ns) and intermediate time (t = 100 ns). Initially $P(\phi)$ is peaked at ϕ = 0 (mixed state) and subsequently evolves into a distribution with two peaks at ±1 (phase coexistence of POPC-rich and PSM-rich domains). As time progresses (t = 100 ns and t = 200 ns), the peaks at ±1 get progressively sharper and the weight at ϕ = 0 diminishes, suggesting that the domain boundaries are getting sharper and that the value of ϕ within the domains approaches the value at equilibrium. To show that we are in the coarsening regime, we need to verify the energy density scaling, which measures the time dependence of the amount of interface separating the two phases (it is more convenient to compute the energy density in Fourier space). This decreases in time, in the dynamical scaling regime, which characterizes nonlinear coarsening, this is expected to go as $\varepsilon \sim t^{-1/z}$, where z = 3, since the order parameter is conserved.[48] Our simulations show that $1/z = 0.30 \pm 0.15$, consistent with this scaling prediction (Figure 2a). As mentioned earlier, this demonstration of coarsening toward the phase-segregated state shows that (i) the homogeneous mixed phase is unstable, (ii) the order parameter within the domains is in local equilibrium, and (iii) the configurations are slowly evolving toward global phase segregation. Of course, to attain this complete phase-segregated state starting from an initial mixed phase takes a very long time for a large-sized system, and has been estimated to be on the microsecond time scale in coarse-grained simulations.[49,50]

To determine physical properties in the global equilibrium state, we would need to run the MD simulation starting from a totally segregated configuration. To make the simulation more efficient, we set the initial partitioning of cholesterol in the two phases consistent with its equilibrium partitioning. This is done by fixing it at the partition coefficient of cholesterol measured in the coarsening regime. To estimate the relative partitioning of cholesterol in the POPC- and PSM-rich regions in the upper leaflet in the coarsening regime, the joint probability distribution of finding a given concentration of PSM with Chol in an xy region (similarly, POPC with Chol) is calculated and shown in Figure 2, b and c. These joint probabilities show that the cholesterol concentration completely correlates with the PSM concentration (i.e., Chol is low (high) when the PSM concentration is low (high)) and completely *anticorrelates* with the POPC concentration (i.e., Chol is low (high) when POPC is high (low)), and shows that cholesterol preferentially partitions in the PSM-rich phase 3 times more than in POPC-rich region (more precisely 2.97:1).

The totally segregated PSM/POPC configuration with cholesterol partitioned in the ratio 3:1 was then used as the initial configuration for the MD runs. Following equilibration, we computed a variety of local and global physical quantities over a time scale of 100 ns, as described below. We calculated the deuterium order parameter S for POPC and PSM, which describes the rigidity of the acyl chain. Using this, the saturated lipid tails of PSM that are in the PSM-enriched domains were found to be more rigid than both the PSM and POPC molecules in the POPC-rich domains. This is reflected in the bimodal distribution of $P(S)$ in Figure 3a. The distinction of the

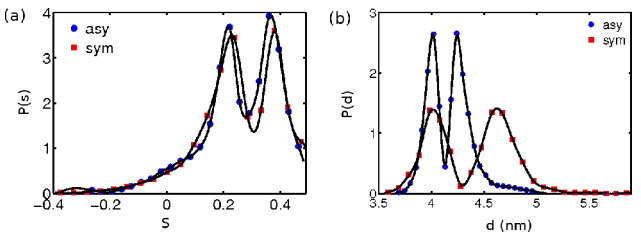

Figure 3. (a) Probability distribution of the deuterium order parameter S in the asymmetric (blue) and symmetric (red) bilayers following equilibration from the fully segregated configuration. Here S of the selected carbons (C5−C7) of POPC and PSM is displayed, after suitable binning in the xy-plane, with the lower branch 0.1−0.26 corresponding to the low partitioning of PSM in the l_d phase and the higher branch 0.35−0.45 corresponding to its enrichment in the l_o phase. (b) Probability distribution of the bilayer thickness d in the asymmetric (blue) and symmetric (red) bilayers following equilibration from the fully segregated configuration. The two distinct peaks in the asymmetric bilayer at 4 and 4.3 nm indicate the coexistence of the l_d and l_o phases. See Materials and Methods.

deuterium order parameter in the two regions indicate that the PSM- and POPC-rich regions may be identified with l_o and l_d phases, respectively. From Figure 3a, it can be seen that the probability distribution of deuterium order parameters in the asymmetric bilayers are comparable to that of symmetric bilayer. These features are replicated in the configurations obtained during coarsening. The probability distribution of S in the coarsening regime is bimodal (Supporting Information, Figure S6A. Further, the segregation of chemical composition is naturally accompanied by an l_o−l_d phase separation, as seen from the spatial variation of S for both asymmetric and symmetric bilayers (Supporting Information, Figure S7). From this spatial distribution, it is visually apparent that the size of l_o domain size (enriched in PSM) is significantly larger in the

dx.doi.org/10.1021/jp3032868 | J. Phys. Chem. B 2012, 116, 13403−13410

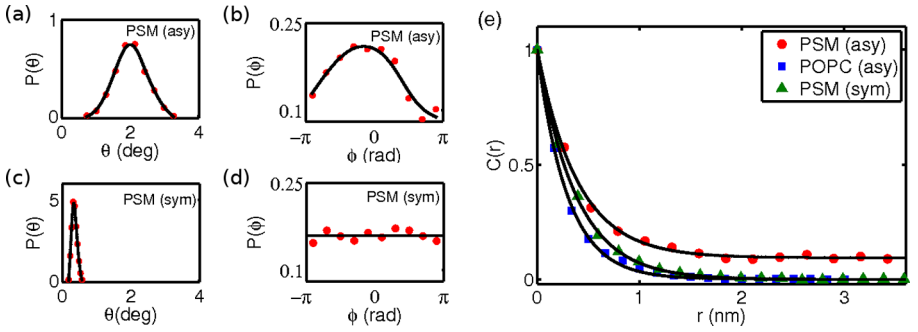

Figure 4. Probability distribution of the coarse-grained tilt angles θ and ϕ of PSM (see text) in (a,b) the asymmetric bilayer, and (c,d) symmetric bilayer, respectively. These data are collected from equilibrium configurations that exhibit complete phase segregation, where the domain size is about half the system size. In the asymmetric ternary bilayer, PSM exhibits a measurable tilt, as evidenced from the distributions of θ and ϕ. In comparison, PSM in the symmetric bilayer shows an absence of tilt—the distribution of θ is peaked at a value close to 0, while the distribution of φ is uniform. (e) The tilt correlation function $C(r) \equiv \langle\phi(r)\phi(0)\rangle$, normalized to its value at $r = 0$, shows an exponential decay to zero for POPC (asymmetric bilayer) and PSM (symmetric bilayer). However, PSM in the asymmetric bilayer shows an exponential decay to a *nonzero value*, demonstrating long-range tilt correlations. The correlation length, defined by the scale at which $C(r)$ decreases to $1/e$ of its value at $r = 0$, can be easily read out, $\xi_{PSM}(sym) = 0.35$ nm, $\xi_{PSM}(asy) = 0.5$ nm and $\xi_{POPC}(asy) = 0.3$ nm.

symmetric bilayer compared to that of asymmetric bilayer, over the time scale measured.

The bilayer thickness d also shows a variation across the phases; the probability distribution of the local bilayer thickness in the fully equilibrated bilayer is displayed in Figure 3b. As with deuterium order parameter, the distribution of bilayer thickness for both the symmetric and asymmetric bilayers is bimodal, corresponding to the (smaller d) POPC-enriched l_d and (larger d) PSM-enriched l_o domains. It is significant that the difference in the bilayer thickness between the l_o and l_d phases in the symmetric bilayer is consistent with recent AFM studies,[53] and is *more than twice compared to asymmetric bilayer*. On probing further, we found that the difference between the mean monolayer thickness in the l_o–l_d domains in the symmetric bilayer (≈0.37 nm) is more than that in the asymmetric bilayer (≈0.358 nm). Even in the coarsening regime, the probability distribution of d is bimodal (Supporting Information, Figure S6A). Further, there is a spatial heterogeneity in the bilayer thickness which follows the l_o–l_d phase segregation (Supporting Information, Figure S7) consistent with the deuterium order parameter results.

Lipid Splay and Tilt. To quantify the relative packing of lipid chains, the amount of splay between the two lipid tails is calculated, in addition to the deuterium order parameter computed above. A tail vector is defined as a vector originating from the carbon of the carbonyl group and pointing to the terminal methyl carbon of a lipid tail. The splay angle ψ is the angle between two such tail vectors of each lipid. The probability distribution, $P(\psi)$, of the splay angle of POPC and PSM is shown in the Supporting Information, Figure S6. Simulation results show that the extent of the splay angle in PSM lipid tails which are predominantly enriched in the l_o-domain is significantly smaller (17°) than that in POPC lipid tails (40°) which predominantly enrich the l_d domain. In addition, the extent of lipid splay in the symmetric and asymmetric bilayers is comparable. Taken together with the deuterium order parameter data, the lipid splay results strongly suggest that the packing fraction of lipids in the PSM-rich phase is higher than that in the POPC-rich phase.

Tilt angle of the lipid tail chain is defined as the orientation of the mean tail vector of the lipid with respect to the local outward normal to the membrane, and is described by two angles (θ,ϕ), the polar and azimuthal angles, respectively. The angle ϕ measures the orientation of the 2d tilt vector, the projection of the tail vector onto the tangent plane, with the x-axis. An accurate determination of the tilt angles of the component lipids is quite involved, since, over short length scales, the local normal to the membrane fluctuates due to molecular protrusion effects. To compute local average tilt, a coarse-graining scale is chosen, which should be more than the protrusion scale and less than the tilt correlation length (which in turn should of course be smaller than the size of the l_o domain). Over this coarse-grained scale, a membrane normal is considered to be along the z-axis. A convenient choice of coarse-graining scale is around a 1 nm^2 (which encompasses ≈3 lipids on an average), for which statistically reliable results can be obtained. For instance, for POPC-only bilayer, the probability distribution of the coarse-grained angle, $P(\theta)$, is peaked about zero, while the distribution $P(\phi)$ is uniform, consistent with the known fact that POPC does not exhibit a tilt at this temperature.[54]

We have used the above procedure to study the local tilt angle distribution of the lipids in the equilibrium phase segregated configurations of the ternary system. The tilt angle distribution of POPC lipids in the symmetric and asymmetric ternary bilayers has a similar distribution as in the case of POPC-only bilayer as seen in Supporting Information, Figure S8. On the other hand, the tilt angle distribution for PSM shows an interesting trend. While PSM in the symmetric bilayer shows no evidence of tilt ($P(\theta)$ is peaked at around 0° and $P(\phi)$ is uniform), PSM in the PSM-rich (l_o) domain of the asymmetric bilayer has a nonzero tilt of around 2.016 ± 0.69°. This small tilt of PSM in the asymmetric bilayer is consistent with the decrease in bilayer thickness of the asymmetric membrane compared to that of symmetric bilayer (see Figure 3b). Tilt angle correlations defined as $C(r) = \langle\phi(r)\phi(0)\rangle$ are computed for POPC and PSM lipid molecules and the results are shown in Figure 4. The correlation functions of the tilt of POPC and PSM (symmetric bilayer) decay exponentially to zero, consistent with the above findings. However, $C(r)$ for PSM in the asymmetric bilayer decays exponentially to a nonzero value, signaling long-range order[51] in PSM molecules in the asymmetric bilayer. This suggests that the asymmetric nature of the bilayer can potentially generate a tilt ordering of PSM molecules in the PSM-rich (l_o) domain.

dx.doi.org/10.1021/jp3032868 | J. Phys. Chem. B 2012, 116, 13403–13410

Previous simulations[12,50,52] and experiments[9,53,55−58] have shown that the thickness of l_o domains is larger than that of the l_d domain. This difference in thickness between l_o and l_d domains gives rise to line tension along the domain boundary.[56] The lipid tails of the l_o domain can be exposed to solvent as a result of such mismatch, which is energetically unfavorable. One of the ways to mitigate such mismatch is for the thicker l_o domain to undergo a small tilt such that the head groups of the two domains can be at the same height. The observed small tilt in the simulations of asymmetric bilayers supports this hypothesis and is consistent with our observation of the smaller monolayer thickness difference of the asymmetric bilayer reported above. Within a Landau theory, the asymmetric bilayer can be thought of as being subjected to a transverse compression, which would naturally lead to a tilt when the lipids are stretched out (as they are in the l_o domain).[59,60]

The existence of a finite tilt and its correlation over long scales, if verified experimentally,[61] could have important consequences for membrane deformation and budding.[62] The tilt vector naturally couples to the local curvature tensor of the membrane, giving rise to anisotropic bending stresses. If the constituent molecules are chiral (as they usually are), then there are additional bending stresses coming from chiral couplings of the tilt and curvature. If strong enough, these bending stresses can induce membrane deformation giving rise to spherical buds or cylindrical tubules.[56,62]

Tagged Particle Diffusion. We have also studied transport quantities such as tagged particle diffusion of the component molecules in the fully segregated equilibrium ternary system. The mean square displacement (MSD) is defined as $\langle \delta r_i(t)^2 \rangle$ of a tagged particle, where $\delta r_i(t) = r_i(t) - r_i(0)$ is the displacement of tagged ith lipid of a given species at time t from its position at $t = 0$. One way to analyze the MSD is to fit it to $\langle \delta r_i(t)^2 \rangle \propto t^{\alpha}$, where α close to 1 could be interpreted as simple diffusion and $\alpha \ll 1$ as subdiffusion. The values of α obtained from fits to the POPC and PSM data taken over a large equilibrium phase-segregated domain in (as)symmetric bilayers are close to 1 and suggest a dynamics close to simple diffusion (Figure 5a).

However, recent single particle tracking experiments of labeled molecules on the cell surface show *marked* deviations from simple diffusion. A variety of explanations have been invoked to explain these data and include molecular crowding and the presence of an actin skeleton fence. Another explanation stems from the lack of evidence for large-scale lipid rafts at the cell surface, and have prompted investigators to suggest that the subresolution lipid domains which are in a process of slow coarsening could be responsible for the slowing down of single-particle transport. This is the motivation to study tagged particle diffusion of component molecules in the coarsening regime.

It should be noted that, even though the membrane composition forms well-defined domains during the process of coarsening, the individual component molecules can traverse across domains. The dynamics of "tagged" component lipids can be monitored by measuring their diffusion coefficients and correlating them with the physical and chemical heterogeneity across the membrane. While computing the MSD, the location of the tagged lipid, whether it is in the POPC-rich (l_d) or PSM-rich (l_o) domain, is monitored by computing the instantaneous deuterium order parameter S of the tagged lipid and the local bilayer thickness. The diffusion analysis is shown in Figure 5b,c. It can be seen that the diffusion coefficient of both PSM and Chol molecules, given by the value of $\langle \delta r_i^2(t) \rangle / 4t$ where it is constant, is different depending on whether the tagged lipid molecule is in the l_o and l_d domain as has been reported in other simulation studies.[50]

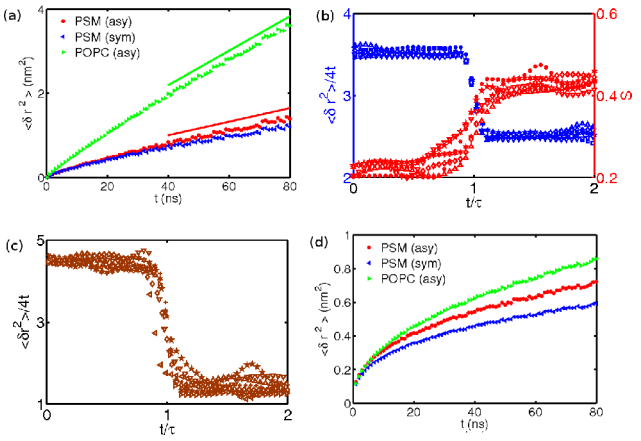

Figure 5. Mean square displacement (MSD) of tagged particles as a function of time collected at high resolution in the ternary bilayer. (a) For the fully segregated equilibrium configuration, the computed MSD vs time data has been fitted to $\langle \delta r_i(t)^2 \rangle \propto t^{\alpha}$: in the asymmetric bilayer $\alpha_{POPC} = 0.89 \pm 0.04$ and $\alpha_{PSM} = 0.82 \pm 0.08$, while in the symmetric bilayer $\alpha_{POPC} = 0.79 \pm 0.03$ and $\alpha_{PSM} = 0.77 \pm 0.02$. Data collected over 80 ns. This analysis shows that the MSD of tagged molecules in large phase-segregated domains at equilibrium is close to simple diffusion (lines drawn for comparison). (b,c) MSD of tagged particles collected at high resolution over short time scales during coarsening in the ternary asymmetric bilayer. Tagged particle diffusion of (b) PSM and (c) Chol in the upper leaflet: statistics collected over six tagged particles, each starting from the l_d domain, shows a data collapse onto a nonlinear crossover scaling curve. The crossover from high to low diffusion occurs at a time τ, computed as the first-passage time of the tagged particle. For PSM, we find that $D_0 = 3.49\ \mu m^2\ s^{-1}$ and $D_\infty = 2.69\ \mu m^2\ s^{-1}$, while for Chol, $D_0 = 4.23\ \mu m^2\ s^{-1}$ and $D_\infty = 1.36\ \mu m^2\ s^{-1}$. Note that in (b) as PSM moves across domains, the deuterium order parameter S of tagged PSM shows a similar crossover, going from ~0.22 (l_d) to ~0.22 (l_o). (d) MSD versus time with fits to $\langle \delta r_i(t)^2 \rangle \propto t^{\alpha}$, for PSM in the asymmetric ($\alpha = 0.39 \pm 0.03$) and symmetric bilayers ($\alpha = 0.35 \pm 0.02$), and POPC and Chol in the upper leaflet of the asymmetric bilayer ($\alpha = 0.45 \pm 0.01$ and 0.41 ± 0.03, respectively), all in the coarsening regime. Note that the α exponent for PSM in the symmetric bilayer is smaller than the asymmetric bilayer, due to the transbilayer coupling. Likewise, the MSD for POPC and Chol in the symmetric ternary bilayer are shown in Supporting Information, Figure S9, for comparison.

Note that only a fraction of tagged molecules will be seen traversing across the domain boundary when measured over a fixed time interval. In the coarsening regime, where the domain sizes are small, this fraction is appreciable. When the tagged PSM or Chol molecules that initially lie in the POPC-rich (l_d) domain cross over to the l_o domain, the local diffusion coefficient crosses over from an early time high value (D_0) to a late time low value (D_∞). For each of the tagged components, a first-passage time, defined as the first time that a tagged molecule residing in a domain moves out of it, is computed. The crossover time τ for each tagged particle is then obtained from such a computed first-passage time. Note that the first passage time, and hence the crossover time, depends on the trajectory of the tagged particle and is therefore a stochastic quantity. Further, the crossover MSD data is collected only for those molecules which cross the domain boundary exactly once.

The MSD is found to obey a crossover scaling relation

dx.doi.org/10.1021/jp3032868 | J. Phys. Chem. B 2012, 116, 13403−13410

$$\langle \delta r^2 \rangle = 4D_0 t F(t/\tau) \quad (1)$$

where the nonlinear scaling function F has the asymptotic form

$$F(t/\tau) = 1 \quad \text{for } t/\tau \ll 1$$
$$= \frac{D_\infty}{D_0} \quad \text{for } t/\tau \gg 1 \quad (2)$$

The data collapse shown in Figure 5, b and c, demonstrates this crossover scaling for PSM and Chol molecules, respectively. Experimentally, the crossover time scale τ can be obtained from the value of t at which the instantaneous $D(t) = (D_0 + D_\infty)/2$, rather than the first-passage time. The values of the diffusion coefficients for PSM molecules (Figure 5b) are in agreement with the experimental findings,[63,64] while the values for Chol molecules (Figure 5b) are slightly lower than those reported in other simulations.[50] This discrepancy can be attributed to the differences in lipid composition of the ternary bilayer used in both the simulations. The difference in the tagged particle diffusion coefficient between the two domains can be attributed to changes in local viscosity (η) and moment of inertia (I) of the particle and to changes in the local density correlations (given by the local partial structure factors, $S_{\alpha\beta}(q)$) with neighboring molecules that the tagged particle experiences as it traverses across the domain. The change in the deuterium order parameter S is used to track the changes in moment of inertia of the tagged molecules. For PSM molecules, this shows a crossover similar to the crossover diffusion, with the value of S being low (high) when the diffusion coefficient is high (low) as seen in Figure 5b. On the other hand, cholesterol being a rigid molecule is unlikely to undergo any conformational change, resulting change in moment of inertia, as it traverses across the domains. Thus, a substantial change in the diffusion coefficient of Chol molecules can be attributed to the changes in viscosity and local density correlations, $S_{\alpha\beta}(q)$, arising from changes in the local environment.

In the context of SPT experiments, if the time scale over which the tagged particle is tracked is large enough so that the particle crosses and recrosses the domains, then one would measure the MSD of $\delta r_i(t) = \int dt'(r_i(t' + t) - r_i(t'))$. For the control pure POPC symmetric bilayer, it is seen that the trajectories are purely diffusive ($\langle \delta r_i(t)^2 \rangle \propto t$) in nature. For the ternary bilayer, however, this MSD would exhibit deviations from true diffusion, which can be characterized by $\langle \delta r_i(t)^2 \rangle \propto t^\alpha$. Figure 5d shows the MSD for the tagged lipids in both the symmetric and asymmetric bilayers and the corresponding values of the exponent α. The value of α obtained for PSM in the asymmetric bilayer ($\alpha \approx 0.39$) is consistent with the experimental value obtained by analyzing recent SPT of labeled PSM on the plasma membrane of epithelial cells, $\alpha \approx 0.3$.[34] The interbilayer coupling in the symmetric ternary system makes the tagged PSM movement slower, as seen by the lower value of $\alpha \approx 0.35$ (see Figure 5d). The tagged particle dynamics of the other lipids in the asymmetric bilayer, viz., POPC and cholesterol, show interesting differences between the two leaflets—typically, the upper leaflet lipids show a smaller α (α = 0.45, 0.41, respectively) than the lower leaflet lipids (α = 0.85, 0.89, respectively).

CONCLUSION

The cell membrane exhibits both lateral and transverse heterogeneity. In this paper, the equilibrium properties of a ternary component asymmetric bilayer membrane system at l_o–l_d phase coexistence are studied using an atomistic MD simulation over a time scale of 220 ns. The asymmetric bilayer considered in this study is composed of POPC, PSM, and cholesterol in the ratio of 1:1:1 in the upper leaflet and POPC and cholesterol in the lower leaflet. The two significant results from this study are (i) cholesterol prefers to be associated with PSM-rich domains (l_o) three times more than in POPC-rich domains (l_d) and (ii) the saturated lipid PSM in the l_o domain exhibits long-range tilt correlations purely as a result of the asymmetry in the bilayer composition (in contrast, the PSM lipid molecules in the symmetric bilayer show no such tilt).

This bilayer asymmetry induced lipid tilt in the l_o domain has important implications to local membrane deformation and hence membrane budding and endocytosis. The existence of a lipid tilt expressed over large scales provides a natural coupling to the local curvature tensor, and results in anisotropic bending stresses at the membrane.[62] Moreover, if the constituent lipids are chiral (as they are in "raft" lipids), then there would be additional bending stresses serving to deform the membrane locally. When the strengths of these couplings are large enough, they can induce the local formation of spherical buds or cylindrical tubules. Recent FRET-based studies of the organization of lipid tethered proteins on the outer surface of living cells, such as GPI-anchored proteins, have shown that they form cholesterol sensitive nanoclusters mediated by the activity of cortical actin.[6,7] These studies imply that there must exist a molecular linkage between the outer leaflet GPI-anchored proteins and cortical actin. The current study will form the basis for further investigations on possible transbilayer interactions between GPI-anchored proteins, PSM and cholesterol, with specific saturated, long chain lipids at the inner leaflet that have potential interactions with actin or actin remodeling proteins.

ASSOCIATED CONTENT

Supporting Information

The first part contains values of force, torque, and surface tension of the mechanically stable symmetric (one component and two components) lipid bilayers. In addition, we have included nine figures describing additional details of the equilibrium pressure, composition, order parameter, bilayer thickness, and tilt profiles of the various model systems we have studied. This material is available free of charge via the Internet at http://pubs.acs.org.

AUTHOR INFORMATION

Corresponding Author

*E-mail: madan@rri.res.in.

Notes

The authors declare no competing financial interest.

ACKNOWLEDGMENTS

We are very grateful to M. Karttunen for generous advice and help on the use of the simulation packages without which this work would not have been possible. We thank R. Sowdhamini for the use of computer facilities, and S. Mayor and V. A. Raghunathan for a critical reading of the manuscript. M.R. acknowledges a grant from HFSP and CEFIPRA 3504-2.

REFERENCES

(1) Devaux, P. F.; Morris, R. *Traffic* **2004**, *5*, 241–246.
(2) Simons, K.; Ikonen, E. *Nature* **1997**, *387*, 569–572.

(3) Lingwood, D.; Simons, K. *Science* **2010**, *327*, 46−50.
(4) Mayor, S.; Rao, M. *Traffic* **2004**, *5*, 231−240.
(5) Hancock, J. F. *Nat. Rev. Mol. Cell Biol.* **2006**, *7*, 456−462.
(6) Sharma, P.; Varma, R.; Sarasij, R. C.; Gousset, K.; Ira; Krishnamoorthy, G.; Rao, M.; Mayor, S. *Cell* **2004**, *166*, 577−589.
(7) Goswami, D.; Gowrishankar, K.; Bilgrami, S.; Ghosh, S.; Raghupathy, R.; Chadda, R.; Vishwakarma, R.; Rao, M.; Mayor, S. *Cell* **2008**, *135*, 1085−1097.
(8) Collins, M. D.; Keller, S. L. *Proc. Natl. Acad. Sci. U.S.A.* **2007**, *105*, 124−128.
(9) Veatch, S. L.; Keller, S. L. *Phys. Rev. Lett.* **2002**, *89*, 268101−268104.
(10) Veatch, S. L.; Keller, S. L. *Biophys. J.* **2003**, *85*, 3074−3083.
(11) Baumgart, T.; Hess, S. T.; Webb, W. W. *Nature* **2003**, *425*, 821−824.
(12) Niemela, P. S.; Ollila, S.; Hyvonen, M. T.; Karttunen, M.; Vattulainen, I. *Plos Comput. Biol.* **2003**, *3*, 0304−0312.
(13) Esteban-Martin, S.; Risselada, H. J.; Salgado, J.; Marrink, S. J. *J. Am. Chem. Soc.* **2009**, *131*, 15194−15202.
(14) Gurtovenko, A. A.; Vattulainen, I. *J. Am. Chem. Soc.* **2007**, *129*, 5358−5359.
(15) Gurtovenko, A. A.; Vattulainen, I. *J. Phys. Chem. B* **2008**, *112*, 4629−4634.
(16) Laradji, M.; Sunil Kumar, P. B. *Phys. Rev. E* **2006**, *73*, 040901.
(17) Wagner, A. J.; Loew, S.; May, S. *Biophys. J.* **2007**, *93*, 4268−4277.
(18) Perlmutter, J. D.; Sachs, J. N. *J. Am. Chem. Soc.* **2011**, *133*, 6563−6577.
(19) Hansen, P. L.; Miao, L.; Ipsen, J. H. *Phys. Rev. E* **1998**, *58*, 2311−2323.
(20) Wallace, E. J.; Hooper, N. M.; Olmsted, P. D. *Biophys. J.* **2005**, *88*, 4072−4083.
(21) Allender, D. W.; Schick, M. *Biophys. J.* **2006**, *91*, 2928−2935.
(22) Egberts, E.; Marrink, S. J.; Berendsen, H. J. C. *Eur. Biophys. J* **1994**, *22*, 423−436.
(23) Berger, O.; Edholm, O.; Jahnig, F. *Biophys. J.* **1997**, *72*, 2002−2013.
(24) Tieleman, D. P.; Forrest, L. R.; Sansom, M. S. P.; Berendsen, H. J. C. *Biochemistry* **1998**, *37*, 17554−17561.
(25) Höltje, M.; Forster, T.; Brandt, B.; Engels, T.; von Rybinski, W.; Höltje, H. D. *Biochim. Biophys. Acta* **2001**, *1511*, 156−167.
(26) Niemelä, P.; Hyvönen, M. T.; Vattulainen, I. *Biophys. J.* **2004**, *87*, 2976−2989.
(27) Zhang, Z.; Bhide, S. Y.; Berkowitz, M. L. *J. Phys. Chem.* **2007**, *111*, 12888−12897.
(28) Khelashvili, G. A.; Scott, H. L. *J. Chem. Phys.* **2004**, *120*, 9841−9847.
(29) Aittoneimi, J.; Niemelä, P. S.; Hyvönen, M. T.; Karttunen, M.; Vattulainen, I. *Biophys. J.* **2007**, *92*, 1125−1137.
(30) Ohvo-Rekila, H. *Prog. Lipid Res.* **2002**, *41*, 66−97.
(31) Rog, T. *Biophys. J.* **2006**, *91*, 3756−3767.
(32) Bhide, S. Y.; Zhang, Z.; Berkowitz, M. L. *Biophys. J.* **2007**, *92*, 1284−1295.
(33) Kusumi, A.; Nakada, C.; Ritchie, K.; Murase, K.; Suzuki, K.; Murakoshi, H.; Kasai, R. S.; Kondo, J.; Fujiwara, T. *Annu. Rev. Biophys. Biomol. Struct.* **2005**, *34*, 351−378.
(34) Sahl, S. J.; Leutenegger, M.; Hilbert, M.; Hell, S. W.; Eggeling, C. *Proc. Natl. Acad. Sci. U.S.A.* **2010**, *107*, 6829−6834.
(35) Tieleman, D. P.; Berendsen, H. J. C. *Biophys. J.* **1998**, *74*, 2786−2801.
(36) Berendsen, H. J. C.; Postma, J. P. M.; van Gunsteren, W. F.; Hermans, J. In *Intermolecular Forces*; Pullman, B., Ed.; D. Riedel Publishing Co.: Dordrecht, The Netherlands, 1981; pp 331−342.
(37) Martinez, L.; Andrade, R.; Birgin, E. G.; Martinez, J. M. *Comput. Chem. J.* **2009**, *30*, 2157−2164.
(38) Koynova, R.; Caffrey, M. *Biochim. Biophys. Acta* **1998**, *1376*, 91−145.
(39) Koynova, R.; Caffrey, M. *Biochim. Biophys. Acta* **1995**, *1255*, 213−236.
(40) de Almeida, R. F. M.; Fedorov, A.; Prieto, M. *Biophys. J.* **2003**, *85*, 2406−2416.
(41) Lindahl, E.; Hess, B.; van der Spoel, D. *J. Mol. Model.* **2001**, *7*, 306−317.
(42) Patra, M.; Karttunen, M.; Hyvonen, M. T.; Falck, E.; Vattulainen, I. *J. Phys. Chem. B* **2004**, *108*, 4485−4494.
(43) Hess, B.; Bekker, H.; Berendsen, H. J. C.; Fraaije, J. G. E. M. *J. Comput. Chem.* **1997**, *18*, 1463−1472.
(44) Miyamoto, S.; Kollman, P. A. *J. Comput. Chem.* **1992**, *13*, 952−962.
(45) Ryckaert, J. P.; Ciccotti, G.; Berendsen, H. J. C. *J. Comput. Phys.* **1977**, *23*, 327−341.
(46) Safran, S. A. *Statistical Mechanics of Membranes and Interfaces*; Addison Wesley: Reading, MA, 1994.
(47) Patra, M. *Eur. Biophys. J.* **2005**, *35*, 79−88.
(48) Bray, A. J. *Adv. Phys.* **2002**, *51*, 481−587.
(49) Pandit, S. A.; Jakonsson, E.; Scott, H. L. *Biophys. J.* **2004**, *87*, 3312−3322.
(50) Risselada, H. J.; Marrink, S. J. *Proc. Natl. Acad. Sci. U.S.A.* **2008**, *105*, 17367−17372.
(51) Chaikin, P. M.; Lubensky, T. C. *Principles of Condensed Matter Physics*; Cambridge University Press: Cambridge, UK, 2000.
(52) Schafer, L. V.; de Jong, D. H.; Holt, A.; Rzepiela, A. J.; de Vries, A. H.; Poolman, B.; Killian, J. A.; Marrink, S. J. *Proc. Natl. Acad. Sci. U.S.A.* **2011**, *108*, 1343−1348.
(53) Rinia, H. A.; Snel, M. M. E.; van der Eerden, J. P. J. M.; de Kruijff, B. *FEBS Lett.* **2001**, *501*, 92−96.
(54) Pan, J.; Mills, T. T.; Nagle, S. T.; Nagle, J. F. *Phys. Rev. Lett.* **2008**, *100*, 198103.
(55) Soni, S. P.; LoCascio, D. S.; Liu, Y.; Williams, J. A.; Bittman, R.; Stillwell, W.; Wassall, S. R. *Biophys. J.* **2008**, *95*, 203−214.
(56) García-Sáez, A. J.; Chiantia, S.; Schwille, P. *J. Biol. Chem.* **2007**, *282*, 33537−33544.
(57) Brown, D. A.; London, E. *J. Biol. Chem.* **2000**, *275*, 17221−17224.
(58) Saslowsky, D. E.; Lawrence, J.; Ren, X.; Brown, D. A.; Henderson, R. M.; Edwardson, J. M. *J. Biol. Chem.* **2002**, *277*, 26966−26970.
(59) Kamal, M. A.; Pal, A.; Raghunathan, V. A.; Rao, M. *EPL* **2011**, *95*, 48004.
(60) Kamal, M. A.; Pal, A.; Raghunathan, V. A.; Rao, M. *Phys. Rev. E* **2012**, *85*, 051701 (9).
(61) Watkins, E. B.; Miller, C. E.; Majewski, J.; Kuhl, T. L. *Proc. Natl. Acad. Sci. U.S.A.* **2011**, *108*, 6975−6980.
(62) Sarasij, R. C.; Mayor, S.; Rao, M. *Biophys. J.* **2007**, *92*, 3140−3158.
(63) Lindblom, G.; Orädd, G.; Filippov, A. *Chem. Phys. Lipids* **2006**, *141*, 179−184.
(64) Pralle, A.; Keller, P.; Florin, E. L.; Simons, K.; Hörber, J. K. *Cell Biol. J.* **2000**, *148*, 997−1008.